MSEL
Modelling in Science Education and Learning

Modelling in Science Education and Learning
Volume 6(3), No. 7, 2013.
Instituto Universitario de Matemática Pura y Aplicada

Modeling Acoustically Driven Microbubbles by Macroscopic Discrete-Mechanical Analogues

Víctor Sánchez-Morcillo, Noé Jiménez, Nuria González
Universitat Politècnica de València
victorsm@upv.es, nojigon@upv.es, nugonsa@epsg.upv.es

Serge Dos Santos, Ayache Bouakaz, Jennifer Chaline
Universitè François-Rabelais (France)
serge.dossantos@univ-tours.fr, ayache.bouakaz@univ-tours.fr, jennifer.chaline@etu.univ-tours.fr

Abstract

La dinámica de sistemas continuos que muestran simetría circular o esférica como gotas, burbujas, o algunas macromoléculas, bajo la influencia de una excitación externa desarrollan patrones de superficie que en muchas situaciones prácticas son difíciles de predecir. En el caso particular de una microburbuja bajo la acción de un campo acústico (agente de contraste ultrasónico), el estudio de la dinámica de la burbuja requiere un complejo modelado incluso para describir los modos de oscilación más simples. Además, debido a la pequeña escala espacio-temporal del problema, el estudio experimental requiere un hardware extremadamente sofisticado y costoso. Por otro lado, la dinámica de muchos sistemas complejos continuos puede ser modelada por medio de agrupaciones de osciladores acoplados. Así, en este trabajo se considera una analogía entre la microburbuja cavitando bajo la acción del campo acústico y un sistema de discreto de osciladores mecánicos excitados paramétricamente. De esta manera, se presenta un estudio teórico y experimental de las inestabilidades de un anillo de péndulos acoplados paramétricamente excitados por una fuerza armónica vertical. Así, el sistema presenta propagación de ondas, exhibiendo no linealidad y dispersión, por lo que una rica dinámica se observa: modos propios, como el modo radial o "breathing mode", dipolar, cuadripolar, etc. y estructuras localizadas como breathers o modos intrínsecos localizados, kinks, etc. Todos ellos han sido observados experimentalmente y numéricamente obtenidos mediante diferencias finitas. A la vista de los resultados, el presente experimento es un excelente banco de pruebas para el estudio de sistemas no lineales en un curso de grado o máster. La presencia de forzamiento paramétrico y pérdidas, así como la interacción entre linealidad y dispersión provoca que el sistema presente la rica dinámica el amplio abanico de fenómenos estudiados de una manera muy visual e intuitiva para el estudiante.

The dynamics of continuous systems that exhibit circular or spherical symmetry like drops, bubbles or some macromolecules, under the influence of some external excitation, develop surface patters that are hard to predict in most practical situations. In the particular case of acoustically driven microbubbles (ultrasound contrast agent), the study of the behavior of the bubble shell requires complex modeling even for describe the most simple oscillation patterns. Furthermore, due to the smallness of the spatio-temporal scale of the problem, an experimental approach requires expensive hardware setup. Despite the complexity of the particular physical problem, the basic dynamical features of some continuous physical systems can be captured by simple models of coupled oscillators. In this work we consider an analogy between a shelled-gas bubble cavitating under the action of an acoustic field and a discrete mechanical system. Thus, we present a theoretical and experimental study of the spatial instabilities of a circular ring of coupled pendulums parametrically driven by a vertical harmonic force. The system is capable of wave propagation and exhibit nonlinearities and dispersion, so manifest rich dynamics: normal oscillation modes (breathing, dipole, quadrupole...) and localized patterns of different types (breathers and kinks) witch are predicted by finite-differences numerical solutions and observed experimentally. On the basis of this analogy, the oscillation patterns and localized modes observed experimentally in acoustically driven bubbles are interpreted and discussed.

Keywords: Dinámica de microburbujas, modos localizados intrínsecos, medios de superficie.
Microbubble dynamics, Intrinsic Localized Modes, surface modes

1 Introduction

Ultrasound contrast agents (UCA) are made of small gas bubbles approximately equal to the size of a red blood cell (radius $R_0 \leq 10\mu m$) used in many common clinical ultrasound systems (enhanced reflectivity imaging, harmonic imaging) as well as new arising medical ultrasound applications (targeted drug and gene delivery, brain-barrier opening) [1][2]. In order to enlarge the life of the free bubbles and stabilize the gas-liquid interface, the gas inside the microbubble is commonly coated into a shell composed by an elastic material (lipids, polymers, albumin, protein)[3] as shown in Figure 1.

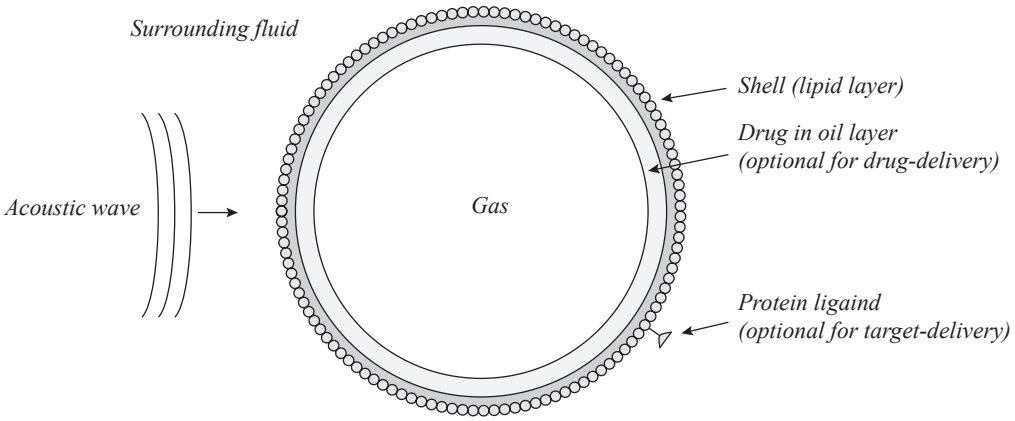

Figure 1: Scheme of a gas-filled microsphere. The gas inside of bubble is coated by a a lipid shell for stabilizing the gas-fluid interface. Optionally, for drug delivery a chemical agent is loaded inside the bubble for transportation. Furthermore, protein ligands can be incorporated on the microbubble surface for targeting the drug to a specific tissue.

Commonly, these microbubbles are injected in the tissue and insonified with an external ultrasound beam. Due to the high difference in the impedance between the bubble and the surrounding fluid, the bubbles act as Rayleigh scatters, increasing the backscattering of the ultrasound beam. Furthermore, due to their high compressibility, the bubbles start to expand and contract during the rarefaction and compression cycles of the pressure wave applied. Because of the nonlinear behavior of these oscillations, the bubble starts to develop non spherical oscillations leading to emission of the fundamental ultrasound frequency but also its harmonics and subharmonics [4].

On this way, the behavior of the microbubbles exhibit rich dynamics that are cumbersome to model and predict. The most simple oscillation is shown in Figure 2, where experimental observations have reported radial mode oscillations. Thus, the initial bubble radius (R_0) exhibits a time variation, the so called "breathing mode", where $R(t) = R_0 + f(t)$.

Furthermore, the bubble present a variety of symmetrical surface patterns (Figure 3), non-spherical (Figure 4) and localized (Figure 5) oscillations, where the radius $R(t) \rightarrow R(t, \theta, \varphi)$ becomes a space dependent function. Finally, at higher external acoustic pressure amplitudes, the bubble start to develop inertial cavitation and collapse, leading to bubble buckling due to high compression pressure and finally shell rupture due to high rarefaction pressures.

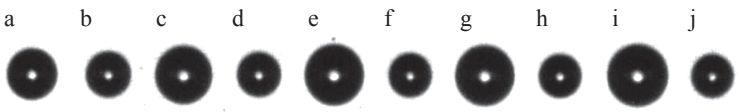

Figure 2: Radial mode oscillation (the so called "breathing mode") as function of time. Volumetric radial mode $m = 0$ for a bubble with a radius of $36\mu m$ driven by a 130 kHz ultrasound beam and captured with a Brandaris high-speed camera. Adapted from [4]

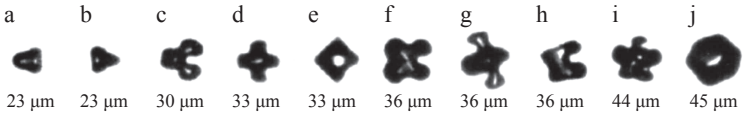

Figure 3: Selection of microbubble oscillation patterns for different radius bubbles recorded by a ultra high frame rate camera, adapted from [4]

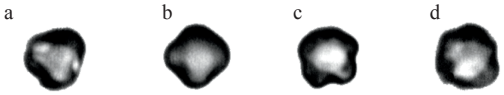

Figure 4: Spherical (a and b) and non-spherical (c and d) coated microbubble oscillation patterns recorded by a ultra high frame rate camera. The forcing frequency was 1.7 MHz for bubbles between 1.5 and 5 μm, adapted from [5]

Figure 5: Localized oscillation mode for a microbubble recorded by a ultra high frame rate camera [4]

The radius of the microbubble can be expanded on the basis of spherical harmonics describing the spatial vibrational modes of the bubble as [6]:

$$R(t,\theta,\varphi) = R(t) + \epsilon \sum_{l=0}^{\infty} \sum_{m=-l}^{l} \alpha_l(t) Y_l^m(\theta,\varphi) \tag{1}$$

In order to study these surface modes a high speed camera of 25 M fps is used in ref [7]. They found that all the modes are axisymmetrical along φ axis, so most of the surface modes of the microbubble can be described by a 2D model by setting $m = 0$.

In this work, an analogy between the shelled microbubble acoustically driven and a circular chain of coupled oscillators parametrically driven by a vertical harmonic force is established and used to study the dynamics of these systems. The analysis and the experiments reveals the existence of Intrinsic Localized Modes (ILM's), similar to those found in other more generic systems of non-linearly vibratory lattices. The observation of ILM in 1D chain of coupled oscillators[8], presenting many similarities with the discrete bubble model, showed to play a role in creating spatio-temporal localized excitations and leading to the breaking of the bubble.

The work is organized as follows: in section 2 the mathematical modeling of the system is described, establishing the analogy between the microbubble and the coupled-pendulum chain (2.1), exposing the governing equations (2.2) and describing a time-domain computational method to obtain numerical solutions (2.3). In section 3 an experimental setup is described and finally in section 4 numerical and experimental results for the coupled pendulum chain are exposed and discussed in section 5.

2 Mathematical Modeling

2.1 The analogy

The radial motion of a bubble under the action of an external pressure field, is well described by the Rayleigh-Plesset equation for the time dependent radius $R(t)$:

$$\rho\left(R\frac{\partial^2 R}{\partial t^2} + \frac{3}{2}\left(\frac{\partial R}{\partial t}\right)^2\right) = p_g - p_0 - p_a(t) - \frac{2\sigma}{R} - \frac{4\mu}{R}\frac{\partial R}{\partial t} \tag{2}$$

where ρ the density of the surrounding fluid, $p_g = (p_0 + 2\sigma/R_0)(R_0/R)^{3\gamma}$ the gas pressure inside the bubble, p_0 is the hydrostatic pressure, R_0 is the equilibrium radius of the bubble, p_a the acoustic pressure, σ the surface tension of the bubble, μ the dynamic viscosity and γ the polytropic exponent. Since acoustic vibrations are typically small in amplitude, one can often linearize the equations to get a simplified description. Linearization consists in assuming

$$R(t) = R_0 + \epsilon r(t) \tag{3}$$

and to describe the coated bubble, the surface tension is modeled by the function:

$$\sigma(R) = \sigma(R_0) + 2\epsilon\gamma\left(\frac{R}{R_0} - 1\right) \tag{4}$$

In this case, it can be shown that the radial variations $r(t)$ can be expressed by a simple driven-damped oscillator as:

$$\frac{\partial^2 r(t)}{\partial t^2} + 2\gamma \frac{\partial r(t)}{\partial t} + \omega_0^2 r(t) = -\frac{p_a(t)}{\rho_l R_0^2} \tag{5}$$

where ω_0 is given by

$$\omega_0^2 = \frac{3}{\rho_l R_0^2}\left(\kappa P_0 + \frac{2(3\kappa - 1)\sigma}{R_0}\right) \tag{6}$$

Thus, the radial vibration of a gas bubble in a fluid is well modeled by a simple harmonic oscillator whose stiffness and mass parameters relate to the properties of the gas and fluid. It is well known that the resonant frequency of the radial mode, known as the Minnaert frequency, is given by

$$f_0 = \frac{1}{2\pi R_0}\sqrt{\frac{3\gamma p_0}{\rho_0}} \tag{7}$$

For a microscopic bubble in water at commonly pressure, this equation reduces to $f_0 R_0 = 3.26$ m/s. Note that a similar scaling relation roughly holds for the proposed macroscopic bubble model.

2.2 Model for the coupled oscillators

A driven-damped chain of coupled pendulums, despite its simplicity, presents a very rich dynamics, and has been used as a toy model for many other physical problems, as a ladder networks of discrete Josephson junctions, charge-density wave-conductors, crystal dislocation in metals, DNA dynamics, and proton conductivity in hydrogen-bonded chains. All these systems are well described by a linear chain. When configured in the form of a circular ring, connecting first and last masses, the chain forms a periodic boundary condition lattice as shown in Figure 6. The coupling of the pendulums is implemented by a nodal junction, which height d governs the coupling factor of the chain. For more details of the construction and modeling of pendulums lattices see ref. [8].

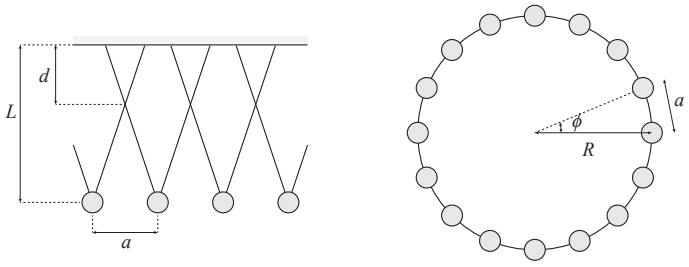

Figure 6: Scheme of the coupled pendulum chain

Thus, considering a pendulum lattice formed by equal masses linearly coupled to their nearest neighbors, and neglecting curvature effects, the motion on the n-th pendulum obeys the

parametrically-driven damped Frenkel-Kontorova equation:

$$\frac{\partial^2\theta_n}{\partial t^2} = -\gamma\frac{\partial\theta_n}{\partial t} - \left(\omega_0^2 + A\cos\left(2\omega t\right)\right)\sin\theta_n + \kappa\left(\theta_{n-1} - 2\theta_n + \theta_{n+1}\right) \tag{8}$$

where θ_n is the angle of the n-th pendulum with the normal, γ is the damping coefficient, $\omega_0 = \sqrt{g/L}$ is the natural frequency of the uncoupled pendulum, g is the acceleration due to Earth's gravity, L is the pendulum length, κ is the coupling constant related on the height d of the junction, and A and ω are the amplitude and the frequency of the parametric excitation.

After linearization, the dispersion relation of the parametrically-excited pendulum chain can be expressed as

$$\left(\frac{\omega_n}{\omega_0}\right)^2 = \frac{1}{1-\eta}\left(1 - \eta cos^2\left(\frac{\pi}{2}\frac{m}{N}\right)\right) \tag{9}$$

where $\eta = d/L \in [0,1]$ measures the strength of the coupling and m is the mode index number and N the number of pendulums. Thus, dispersion relation is bounded by the lower cutoff frequency $\omega_l = \sqrt{g/L}$ and upper cutoff frequency $\omega_u = \sqrt{g/(L-d)}$ which corresponds to the natural frequency of pendulum oscillating either from the rigid support or from the knot, respectively (Figure 7).

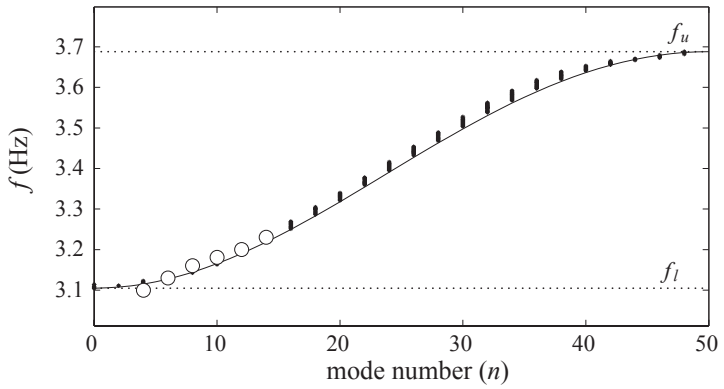

Figure 7: Dispersion relation for the coupled pendulum chain, showing the good agreement between the theoretical (solid line), numerical (black dots) and experimental (white dots) results.

2.3 Numerical solution of coupled oscillators

In order to obtain a solution of the coupled pendulum motion equation, finite differences are applied to partial differential operators of eq. 8. Thus, time is uniform discretized as $t = i \cdot \Delta t$, where Δt is the temporal step and i is the discrete time index. On this way, centered finite differences are applied to second order partial differential operators and forward finite differences are applied to first order partial differential operators. Then, the discrete equation can be written as:

$$\begin{aligned}\frac{\theta_n^{i-1} - 2\theta_n^i + \theta_n^{i+1}}{\Delta t^2} \;=\; & -\gamma\frac{\theta_n^i - \theta_n^{i-1}}{\Delta t} \\ & -\left(\omega_0^2 + \eta\cos\left(2\omega t\right)\right)\sin\theta_n^i \\ & +\kappa\left(\theta_{n-1}^i - 2\theta_n^i + \theta_{n+1}^i\right)\end{aligned} \tag{10}$$

The past values (θ_n^{i-1}) and the actual state of the chain (θ_n^i) are defined by the initial conditions of the pendulum ring, so only the future values (θ_n^{i+1}) are unknown in eq. 10. Thus, in order to solve the discrete equation, a "leap-frog" time steeping is applied, so the solution for θ_n^{i+1} can be expressed as:

$$\begin{aligned} \theta_n^{i+1} &= -\theta_n^{i-1} + 2\theta_n^i \\ &\quad -\Delta t\gamma\left(\theta_n^i - \theta_n^{i-1}\right) \\ &\quad -\Delta t^2\left(\omega_0^2 + \eta\cos\left(2\omega t\right)\right)\sin\theta_n^i \\ &\quad +\Delta t^2\kappa\left(\theta_{n-1}^i - 2\theta_n^i + \theta_{n+1}^i\right) \end{aligned} \tag{11}$$

This equation is solved for the N pendulum and for $i = 0, 1, 2, \cdots, T/\Delta t$ where T is the total time of the prediction. In this way, after solving this equation once for $i = 0$ a time step is advanced $i' = 1$, so the new past value becomes the actual value ($\theta_n^{i'-1} = \theta_n^i$), and the new actual value is assigned with the recently calculated future value ($\theta_n^{i'} = \theta_n^{i+1}$). The periodic boundary conditions for the ring of pendulums implies that for solving the first pendulum ($n = 1$):

$$\begin{aligned} \theta_1^{i+1} &= -\theta_1^{i-1} + 2\theta_1^i \\ &\quad -\Delta t\gamma\left(\theta_1^i - \theta_1^{i-1}\right) \\ &\quad -\Delta t^2\left(\omega_0^2 + \eta\cos\left(2\omega t\right)\right)\sin\theta_1^i \\ &\quad +\Delta t^2\kappa\left(\theta_N^i - 2\theta_1^i + \theta_2^i\right) \end{aligned} \tag{12}$$

And for solving the last pendulum ($n = N$):

$$\theta_N^{i+1} = \theta_1^{i+1} \tag{13}$$

3 Experimental Setup

The coupled pendulum chain is built by a set of $N = 50$ pendulums of $L = 103$ mm length, and a mass of 5 g disposed around a ring of $R = 330$ mm radius. The distance between pendulums is $a = 50$ mm and the junction according the Figure 6 is done by a knot at $d = 30$ mm.

Thus, the natural frequency of pendulum oscillating from the rigid support is $f_l = 3.1$ Hz (lower cutoff mode), and the natural frequency of pendulum oscillating from the knot is $f_u = 3.69$ Hz (upper cutoff mode).

The parametric excitation is exerted by a vertical displacement by means of a 18" audio subwoofer (*Fostex L363, Foster Electric Co. Rochester, MN, USA*) driven by a harmonic low frequency signal. The low frequency signal is generated by a arbitrary function generator (*Agilent 33220A, Agilent Technologies Inc. Loveland, CO, USA*), amplified by an audio amplifier (*Beringer EP2500, Behringer International GmbH, Germany*) and then connected to the 8 ohms input of the loudspeaker. The subwoofer is facing up on a rigid table and the pendulum ring lies directly on the active diaphragm cone of the loudspeaker as shown in Figure 8.

The duration of the tests was 100 s, and the frequency of the excitation was in the range $(3.00, 4.10)$ Hz. The oscillation patterns of the ring were recorded by means of web-cam recorder

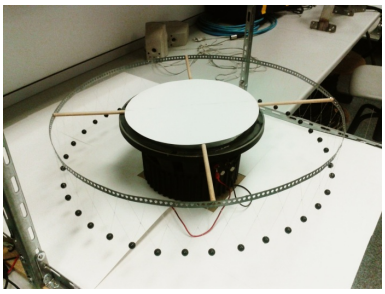

Figure 8: Experimental set-up of the parametrically excited coupled pendulum chain. The excitation of the chain is exerted by a vertical displacement by means of 18" audio subwoofer driven by a harmonic low frequency signal.

placed on the top of the system. Thus, images of 720/480 pixels were acquired at 30 frames per second, leading to a minimum of 7.5 images per cycle of oscillation.

The initial excitation of the chain was exerted manually by moving one of the pendulum. Therefore, this implies a high bandwidth as initial condition of the chain.

4 Results

Both simulation and experimental results shows a variety of patterns in the ring of pendulum: oscillation modes, non-propagating solitons, kinks and other structures like asymmetric modes.

4.1 Breathing mode ($m = 0$)

A singular vibration mode of the system is the mode $m = 0$, the so called "breathing mode" (don't mistake with a breather or a non-propagating soliton). The breathing mode is predicted by the most simple bubble modes, and in most applications the bubble is assumed to oscillate in this pattern. For the numerical simulations the breathing mode appears at $f = 3.35$ Hz, and for the experiment at $f = 3.32$ Hz.

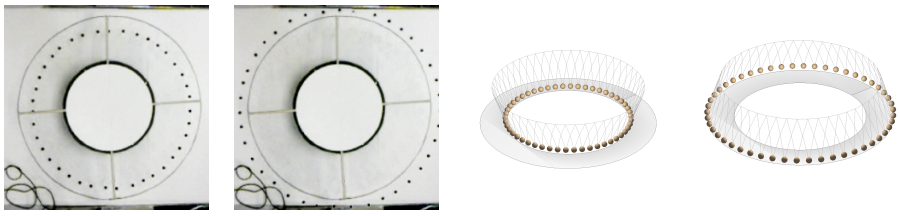

(a) (b) (c) (d)

Figure 9: Experimental (a), (b), and numerical (c), (d),results for the breating mode $m = 0$ of the ring of coupled pendulums

4.2 Eigenmodes

The parametrically excited chain shows a selection of modes from $m = 1, 2, 3, \cdots, N/2$. Fig. 10 shows the numerical solution and the experimental result for $m = 2, 3, 4, 7$, where the excitation

frequencies were 3.10, 3.13, 3.18 and 3.23 Hz respectively. This modes are also plotted in the dispersion relation of Figure 7, where the numerical, theoretical and experimental results agrees.

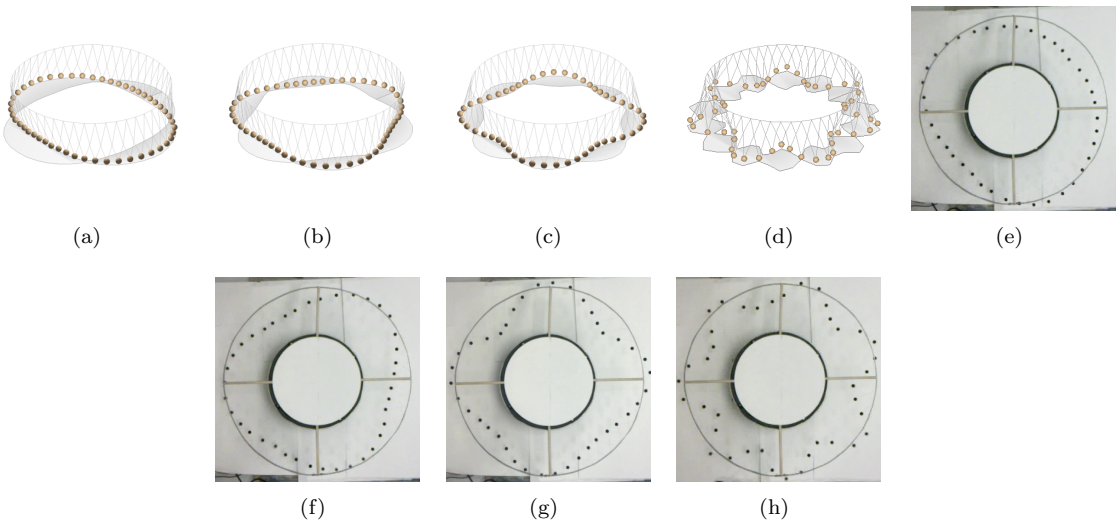

(a) (b) (c) (d) (e)

(f) (g) (h)

Figure 10: Numerical (a), (b), (c), (d) and experimental results (e), (f), (g), (h) for the modes $m = (2, 3, 4, 7)$ respectively

4.3 Lower cutoff modes

In addition to the vibration modes of the ring other exotic patterns are found in the system. Localized modes are found as a stable solutions of the chain at excitation frequencies slightly below $2\omega_l$. Thus, Figure 11 shows experimental results for a excitation of $f = 3.03$ Hz where a non-propagating soliton is observed. Numerical results for an excitation of $f = 3.04$ are shown in 12. Figure 13 shows a scheme of the unwarped ring where the phase of the localized mode is represented.

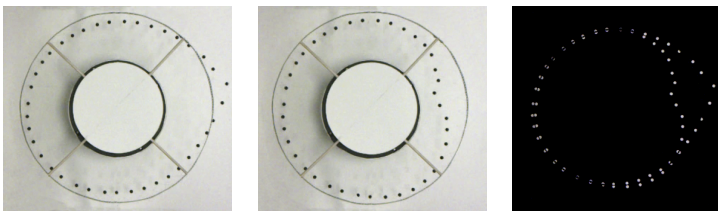

(a) (b) (c)

Figure 11: Experimental results of a localized mode (breather) for $f = 3.03$ Hz. Image (c) is the difference of the phases (a), (b)

Another type of soliton is formed in the chain at $f = 3.05$ Hz. In this case, two stable localized structures are formed as Figure 14 shows. A bound state of two breathers oscillating with opposite phases is observed, the fig 15 shows a scheme of the unwarped ring where the phases of the localized modes are represented.

(a) (b)

Figure 12: Numerical results of a localized mode (breather) for a excitation of $f = 3.04$ Hz

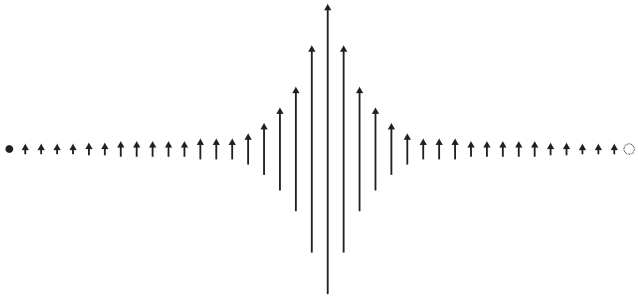

Figure 13: Scheme of the localized mode of the unwarped ring. Here, arrows represent the phase off the pendulum oscillations and dots the nodes.

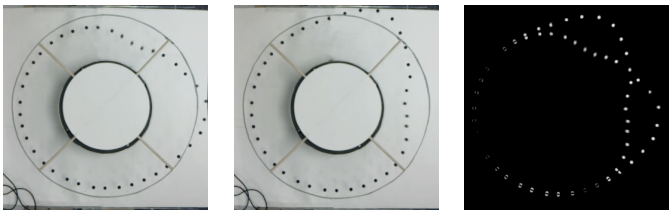

(a) (b) (c)

Figure 14: Experimental results of a double localized mode. Image (c) is the difference of the phases (a), (b)

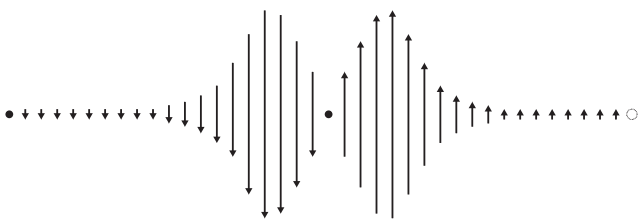

Figure 15: Scheme of the double localized structure of the unwarped ring. Here, arrows represent the phase off the pendulum oscillations and dots the nodes.

4.4 Upper cutoff modes

In the upper cutoff region, kink modes are found as a stable solutions of the chain at excitation frequencies above $2\omega_u$. Thus, an upper cutoff kink is observed both numerically (Figure 17) and experimentally (Figure 16) for $f = 3.99$ Hz. Figure 18 is useful to observe the the kink phase distribution.

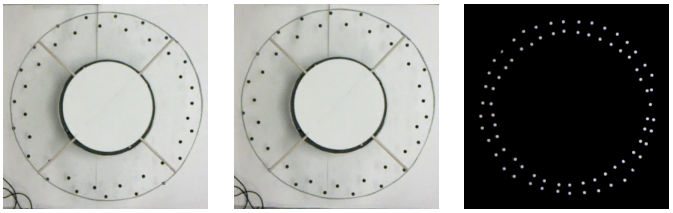

(a) (b) (c)

Figure 16: Experimental results showing a kink in the ring for an excitation frequency of $f = 3.99$ Hz. Image (c) is the difference of the phases (a), (b)

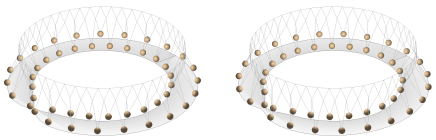

(a) (b)

Figure 17: Numerical results for the upper cutoff limit kink

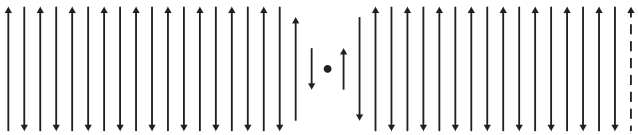

Figure 18: Scheme of the kink pattern of the unwarped ring. Here, arrows represent the phase off the pendulum oscillations and dots the nodes.

In addition, another type of breather is observed for $f = 4.09$ Hz, where a localized structure is formed with the pendulums oscillating in opposite phases as Figure 19 and Figure 20.

However, solutions do not find an equivalent in real bubbles (neighbor particles oscillate in anti-phase).

5 Conclusions

In this paper a ring of coupled oscillators is proposed as a discrete-mechanical analogue of acoustically driven shelled microbubbles. However, despite the relevance of the results for the field of ultrasound contrast agents, the proposed model is a good candidate for be an illustrative example of how the combined effects of nonlinearity and dispersion leads to the exposed rich dynamics of the system. Thus, the simple construction of the pendulums ring

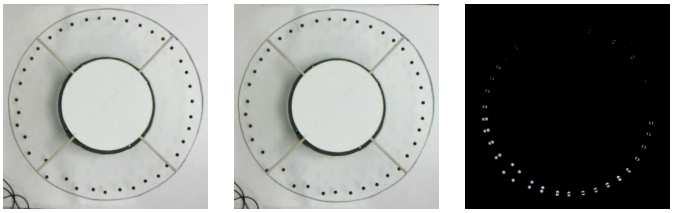

(a) (b) (c)

Figure 19: Experimental results of a anti-phase breather-type mode for $f = 4.09$ Hz. Image (c) is the difference of the phases (a), (b)

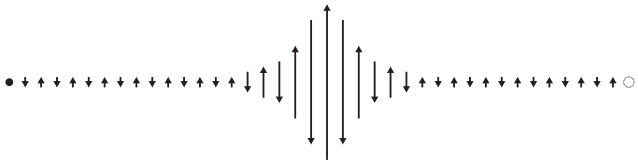

Figure 20: Scheme of the anti-phase breather structure of the unwarped ring. Here, arrows represent the phase off the pendulum oscillations and dots the nodes.

and the cheap electronics makes this experimental setup suitable for a lecture. Furthermore, the numerical solution of the model is also straightforward to programming and the results effortless to interpret.

Acknowledgment

The authors acknowledge financial support from the Spanish Ministry of Science and Innovation and European Union FEDER through project FIS2011-29731-C02-02.

References

[1] K. Ferrara, R. Pollard, M. Borden. Ultrasound microbubble contrast agents: Fundamentals and application to gene and drug delivery. *Annual Review of Biomedical Engineering*, **9**(1), 415–447 (2007).

[2] S. Qin, C.F. Caskey, K.W. Ferrara. Ultrasound contrast microbubbles in imaging and therapy: physical principles and engineering. *Physics in Medicine and Biology*, **54**(6):R27 (2009).

[3] S.R. Sirsi, M.A. Borden. Microbubble compositions, properties and biomedical applications. *Bubble Science, Engineering & Technology*, **1**(1-2), 3–17 (2009).

[4] M. Versluis, D. E. Goertz, P. Palanchon, I.L. Heitman, S.M. van der Meer, B. Dollet, N. de Jong, D. Lohse. Microbubble shape oscillations excited through ultrasonic parametric driving. *Phys. Rev. E*, **82**(2):026321, August (2010).

[5] B. Dollet, S.M. van der Meer, V. Garbin, N. de Jong, D. Lohse, M. Versluis. Nonspherical oscillations of ultrasound contrast agent microbubbles. *Ultrasound in Medicine & Biology*, **34**(9), 1465–1473, (2008).

[6] M. S. Plesset. On the stability of fluid flows with spherical symmetry. *Journal of Applied Physics*, **25**(1):, 96–98 (1954).

[7] M. Versluis, S. M. van der Meer, D. Lohse, P. Palanchon, D. Goertz, C. T. Chin, N. de Jong. Microbubble surface modes. In *Proceedings of the 2004 IEEE Ultrasonics Symposium*, **1**(3), 207–209 (2004).

[8] B. C. Denardo. *Observations of Nonpropagating Oscillatory Solitons*. PhD thesis, University of California, Los Angeles, (1990).